LRP 516/95 May 1995

SHEATH IMPEDANCE EFFECTS IN VERY HIGH FREQUENCY PLASMA EXPERIMENTS

W. Schwarzenbach, A.A. Howling, M. Fivaz,
S. Brunner, and Ch. Hollenstein

submitted for publication in

Journal of Vacuum Science
and Technology A

Sheath Impedance Effects in Very High Frequency Plasma Experiments

W. Schwarzenbach, A. A. Howling*, M. Fivaz, S. Brunner, and Ch. Hollenstein

Centre de Recherches en Physique des Plasmas
Ecole Polytechnique Fédérale Lausanne,
Av. des Bains 21, CH-1007 Lausanne, Switzerland

The frequency dependence (13.56 MHz to 70 MHz) of the ion energy distribution at the ground electrode was measured by mass spectrometry in a symmetrical capacitive argon discharge. Reduced sheath impedance at Very High Frequency allows high levels of plasma power and substrate ion flux whilst maintaining low levels of ion energy and electrode voltage. The lower limit of ion bombardment energy is fixed by the sheath floating potential at high frequency, in contrast to low frequencies where only the rf voltage amplitude is determinant. The capacitive sheaths are thinner at high frequencies which accentuates the high frequency reduction in sheath impedance. It is argued that the frequency dependence of sheath impedance is responsible for the principal characteristics of Very High Frequency plasmas. The measurements are summarised by simple physical descriptions and compared with a Particle-In-Cell simulation.

* Author to whom correspondence should be addressed

I. INTRODUCTION

The interest of Very High Frequency (VHF: 30 - 300 MHz) plasma processing, compared with the conventional 13.56 MHz frequency, has been demonstrated by experiment[1-10] and modelling.[2,5,11-15] Measurements and/or scaling laws from numerical simulation have shown high deposition rates,[1,3,6] improved uniformity[3,13] and reduced stress[15] of the deposited films, and thinner sheaths[8,12,13,16,17] with low energy,[3,5-7,12] high flux[5-7,12] ion bombardment at the substrate. VHF plasmas have also proved advantageous for reactive ion etching[7] and microcrystalline silicon deposition.[9,10]

Ion bombardment is necessary for surface species reactivity[18,19] but can damage the film during plasma deposition[19] or etching[20] by high-energy ion impact caused by acceleration across high-voltage sheaths. The sheath voltage can be controlled independently of the rf voltage and power by varying the self-bias (inherently requiring electrode asymmetry[21] which is impractical for uniform, large area deposition), by an imposed dc bias (not recommended for plasma processing due to a risk of dielectric breakdown[21,22]), and in triode[19] or magnetron devices (incurring scale-up problems[5]). Ion bombardment control with the VHF technique avoids these difficulties provided that the rf frequency and electrode voltage can be suitably chosen.[3-6,12,14]

In this paper, we investigate the sheaths and ion flux in VHF discharges to gauge the extent to which VHF behavior can be explained by the sheaths,[6] before invoking frequency effects on the electron temperature or distribution function.[2,23] The frequency dependence of ion bombardment has previously been studied below 13.56 MHz,[22] whereas quantitative experimental data for ion energy and flux in VHF plasma deposition has been lacking until recently.[6]

In this work, the ion distribution function was monitored by quadrupole spectrometry at the ground electrode for a range of excitation frequency (13.56 to 70 MHz), rf electrode voltage (10 to 210 V amplitude), and plasma power (1 to 14 W). The discharge studied was symmetric (self-bias $\approx$ 0 V[22]) for all

parameters) to avoid any extraneous reactor geometry effects due to frequency-dependent self-bias.[7,24] This symmetry also permitted comparison with a 1-D Particle-In-Cell (PIC) code[25] and is relevant to large-area-deposition plasma reactors. Argon plasmas involve only one neutral and one ionic majority species and so avoid radical chemistry complications. This simple discharge type was chosen with the aim of investigating the inherent properties of the VHF technique which are not gas-, process-, or machine-dependent.

II. DESCRIPTION OF THE EXPERIMENT AND NUMERICAL SIMULATION

The rf capacitive reactor shown in Figure 1 comprised two cylindrical stainless steel electrodes, diameter 130 mm and a 30 mm fixed electrode gap, with the upper electrode and the walls of the chamber grounded. The argon pressure was 0.1 Torr with a 50 sccm flow throughput to maintain gas purity. The lower rf electrode was capacitively coupled via a π matching box and rf power-meter to a wideband rf-amplifier and signal generator. A passive probe mounted on the back face of the rf electrode was used to measure the rf voltage amplitude V_{rf} and electrode self-bias V_{dc}. The probe and its oscilloscope were integral components of the reactor and so introduced no perturbation to the system impedance. The areas of the ground and rf electrodes were equalised by confining the plasma within concentric stainless steel screens, as shown in Fig. 1, to obtain approximately zero self-bias of the rf electrode ($V_{dc} / V_{rf} < 5\%$ for all experiments); the discharge was thus considered to be symmetric.

A Hiden Analytical Limited[26] Plasma Monitor HAL-EQP 500 was used to measure the mass and energy of ions impinging on the ground electrode at the electrode axis (Fig. 1). The ions entered the monitor first through a 5 mm diameter orifice in the ground electrode and then through a 100 μm aperture in the negatively-biased (-50 V) extractor head. A 45° electrostatic energy analyser selects the ion energy before the quadrupole mass filter and also eliminates ions

which have inelastic collisions after crossing the ground plane of the electrode surface.

The code XPDP1[25] is a 1D Particle-In-Cell (PIC) and Monte-Carlo collision code applicable to a symmetric plasma geometry. It provides a fully-kinetic representation for plasma ions and electrons. Cross-section models for ion-neutral and electron-neutral collisions in an argon plasma simulate charge exchange collisions, ionization, excitation and elastic scattering. This code was implemented on a MUSIC[17] parallel computer allowing long simulations (10^3 rf periods) of the experiment. The rf electrode voltage in the simulation was taken from the experimentally-measured applied voltage corresponding to the required plasma conditions to be simulated.

III. RESULTS

A. Ion energy distributions and determination of the time-averaged plasma potential

The argon ion flux energy distributions in Fig. 2 were obtained by experiment and simulation for the same rf frequency and electrode voltage. The dispersion of the Ar^+ distribution is caused by symmetric resonant charge exchange in the sheath with argon neutrals.[27] The peaks in intensity[12,17] are due to the interaction of the oscillating rf potential and charge exchange collisions[28] as the ions cross the sheath during several rf periods. This structure is visible on both the experimental and simulation data and can be used to deduce the time-averaged sheath potential profile.[17]

The ArH^+ ion, a minority species formed by Ar^+ reacting with hydrogen from residual water in the reactor, does not suffer charge exchange because its equivalent neutral does not exist and most reach the electrode with no inelastic collisions. Their energy distribution is a single peak since the ions only respond to the time-averaged sheath potential[22] as they cross the sheath during several rf cycles: the rf frequency is between the ion and electron plasma frequencies so

that only the electrons can follow the time-varying rf fields. Both the maximum Ar^+ energy (for those Ar^+ ions which cross the sheath without collision) and the ArH^+ peak therefore correspond to the time-averaged sheath voltage at the ground electrode which equals the time-averaged plasma potential $\overline{V_p}$. The well-defined ArH^+ peak is used similarly to Köhler *et al* [21] for the experimental estimate of $\overline{V_p}$ and the PIC simulation gives $\overline{V_p}$ as an output parameter.

B. Ion energy as a function of rf frequency and rf voltage

For rf capacitively-coupled discharges with asymmetric electrodes, the rf electrode voltage is $V(t) = V_{dc} + V_{rf}\sin\omega t$, where V_{rf} is the rf voltage amplitude and V_{dc} is the dc self-bias voltage[21,22] given by

$$V_{dc} = V_{rf}(C_t - C_w)/(C_t + C_w),$$

where C_t and C_w are the sheath capacitances at the rf and ground electrode respectively. In our reactor, the rf and ground electrode areas were symmetrically adjusted (see Fig. 1) to obtain $V_{dc} = 0$, whereupon $C_t = C_w$ and the plasma potential $V_p(t)$ is of equal amplitude and in antiphase with respect to each electrode. The time-averaged plasma potential $\overline{V_p}$ for an equivalent circuit sheath description is then given by[21,22]:

$$\overline{V_p} = K V_{rf} + \Delta V(T_e, V_{rf}) \qquad (V_{dc} = 0) \qquad (1)$$

where K is a constant which depends only on the waveform $V_p(t)$ of the plasma potential and is in the range $1/\pi \leq K \leq 1/2$; the upper and lower limits correspond to sheaths which are purely capacitive (sinusoidal $V_p(t)$) and resistive (half-wave-rectified $V_p(t)$), respectively.[21,22] The term $\Delta V(T_e, V_{rf})$ is a correction to the equivalent circuit model[21] to account for residual differences compared with electron temperature and self-rectification effects.[29,30] These latter effects arise naturally in a plasma description where the time-averaged electron/ion currents at each electrode cancels giving[29,31,32]:

$$\overline{V_p} = V_f + (kT_e/e)\ln\left(I_o(eV_{rf}/2kT_e)\right) \qquad (2)$$

for a sinusoidally-varying sheath potential of amplitude $V_{rf}/2$, where I_o denotes the zeroth order modified Bessel function.[29] In the limit of small eV_{rf}/kT_e, the plasma potential is positive with respect to the electrode by the floating potential[33] $V_f \approx 16$ V in argon, taking $kT_e/e \approx 3$ eV. In the limit of large eV_{rf}/kT_e, the aymptotic expansion of I_o gives[21,31]:

$$\overline{V_p} = V_f + V_{rf}/2 - (kT_e/2e)\ln(2\pi(eV_{rf}/2kT_e)), \qquad (3)$$

which is approximately linear with unity gradient in Fig. 3.

The $\overline{V_p}$ *vs* V_{rf} data for different rf frequencies are compared with Eqs. (1) and (2) in Fig. 3, where the ArH^+ energy was used for the measurement of $\overline{V_p}$. Comparable rf power ranges were used at each frequency, and the rf power corresponding to each V_{rf} value is shown in Fig. 4(a). There is very good agreement with the plasma description of Eq. (2), using the same electron temperature $kT_e/e \approx 3$ eV irrespective of rf power or excitation frequency. This is also experimental confirmation of the recent approach of Wang (see Ref. 32 with $\alpha = 1/2$ for symmetric electrodes) in applying the Garscadden and Emeleus[29] expression to capacitive discharges. Both experiment and simulation in Fig. 3 show that the sheaths behave capacitively at these frequencies (the discrepancy between experiment and simulation may be due to systematic errors in the measurement and/or imprecision in the differential cross-sections used in the PIC code); the PIC simulation and an analytical solution for rf sheaths[34] also demonstrate sinusoidally-varying sheath potentials with only a weak contribution from higher harmonics. This result is independent of the value of sheath capacitance, plasma power or rf frequency and agrees with other work[16,35,36] that the displacement current dominates the charge-carried current in the sheaths.

From Fig. 3 and Eq.(3), the maximum ion energy ($\approx e\overline{V_p}$) therefore increases almost linearly at high values of applied rf voltage V_{rf}, as shown also by scaling laws,[5,12] but tends to a non-zero energy eV_f in the limit of small V_{rf}. This lower limit of ion energy is not of practical importance in capacitive symmetric discharges below 13.56 MHz[22] because the discharge power density at

low frequency must be very small for V_{rf} to become comparable to V_f. VHF operation allows access to this region because V_{rf} can reach sufficiently low levels even with significant plasma power due to reduced capacitive sheath impedance at high frequencies. In the VHF régime, the plasma is sustained even with V_{rf} smaller than the argon ionisation potential[5] of 15.76 eV. The maximum ion energy at constant V_{rf} is independent of frequency,[12] to within experimental accuracy, as expected since all plasma potential waveforms $V_p(t)$ are the same (sinusoidal) for the range of frequencies studied here.

Fig. 4(a) shows the plasma power range used at frequencies corresponding to the experimental data in Fig. 3. At 13.56 MHz the maximum power used was 3 W because the ion energy at higher powers exceeded the 106 eV energy range of the mass spectrometer. The plasma power P_p was estimated to within 15% accuracy[15] by subtracting the input power measured without plasma at a given electrode voltage, from the input power with plasma at the same voltage.[3,38] The results are therefore independent of machine-dependent network losses and so are valid for any reactor with equivalent dimensions because V_{rf} and P_p are one-to-one functions for given plasma parameters (including rf frequency); that is, the plasma is unchanged by transfer to other reactors where the external circuit can maintain the same V_{rf} across the plasma/sheath system. In fact, the results are applicable for the same plasma parameters to any symmetric reactor with the same electrode gap, provided that the plasma power and ion flux are scaled with the electrode area.

The approximate proportionality of V_{rf}^2 and P_p in Fig. 4(a) (observed also by Andries *et al* [39]) along with the capacitive sheath behavior deduced from Fig. 3, suggests a commonly-used equivalent series circuit of a resistive plasma (resistance R) bounded by two capacitive sheaths ($C_t = C_w = C$ at each electrode for this symmetric plasma). The proportionality may be in part fortuitous because this simple model does not account for ion power gained from the V_{rf} source[36]; however this contribution is small compared with dissipation in

the bulk plasma at the low V_{rf} values[36] associated with VHF frequencies. The measured constant of proportionality between V_{rf}^2 and P_p as a function of rf frequency is shown in Fig. 4(b) for all the data of Fig. 3. For the C - R - C circuit, where C and R may each depend on the frequency, this relation is:

$$V_{rf}^2/P_p = \left(R^2 + (2/\omega C)^2\right)/R \approx 4/\omega^2 C^2 R = f(\omega) \qquad (4)$$

since the plasma resistance R is much smaller than the sheath impedance $1/\omega C$ even at 70 MHz.[8] A power law fit to the data in Fig. 4(b) gives $f(\omega) \propto \omega^{-2.4\pm0.2}$. An inverse square frequency-dependence would correspond to constant C and R (and agree with simulations[5,12,14]). However, the sheath thickness d_s is well-documented[5,7,8,12,16,17] to decrease with excitation frequency (see also Section III.D) so that $C = \varepsilon_o/d_s$ (per unit electrode area) increases. Since the sheath impedance is $1/\omega C$, any high frequency effect is therefore accentuated by this simultaneous increase in C. The ωC term should be accounted for before any frequency-dependence of the bulk plasma impedance R is invoked. Eq. (4) shows why the plasma power P_p increases strongly with rf frequency for constant V_{rf}, physically because the sheath capacitive impedance is 'short-circuited' at VHF and more rf voltage appears directly across the bulk plasma. Equivalently, the power factor $\cos\phi \approx \omega CR$ (where $R < 1/\omega C$) increases because the total impedance becomes less reactive. For the same reason, the rf amplitude of the bulk plasma electron current, which approximately equals the sheath displacement current $(\omega C)V_{rf}$, also increases with frequency.

An additional representation is shown in Fig. 5 by varying the frequency at constant plasma power. The electrode voltage and ion energy, by experiment and simulation, both decrease with excitation frequency but the ion energy reaches a lower limit determined by the floating potential whereas V_{rf} continues to fall - this limit was overlooked in an earlier paper.[3] This means that, for a given rf power density, there is a corresponding frequency above which no significant further reduction in ion energy is obtained (approximately 70 MHz in Fig. 5);

this frequency being the same for any symmetric reactor with the same electrode gap and plasma parameters.

C. Ion flux as a function of rf frequency and rf voltage

Since low-energy ion bombardment can be beneficial for plasma deposition[18,19] and reactive ion etching,[20] it is important to produce a sufficient flux of these ions. Surface damage during plasma deposition occurs above a threshold in ion energy, and so the following experiments evaluate the influence of excitation frequency on ion flux for a fixed upper limit of bombardment energy.

Fig. 6 shows the Ar^+ ion energy distributions, normalised to the total flux, for a maximum ion energy of 29 eV obtained by adjusting the rf power at each frequency. From Fig. 3, this is closely equivalent to using the same V_{rf} as the frequency is varied. The mean energy of the ion flux almost doubles in passing from 13.56 MHz to 70 MHz (see Fig. 7), in general agreement with simulations.[5,12] This is due to the lower probability of charge exchange collisions in the thinner sheaths at high frequency, and is demonstrated in Fig. 7 by the ratios of sheath width to mean free path obtained by fitting the Davis and Vanderslice distribution function[27] to the data[17] of Fig. 6.

The frequency-dependence of the total ion flux integrated over energy is given in Fig. 8 for constant maximum energies of 29 and 39 eV. At 70 MHz, the measured fluxes are a factor 30 more intense than at 13.56 MHz, with a $f^{2.1\pm0.2}$ power law dependence (in agreement with simulations[5,12]) and no indication of saturation with frequency.

The relationship between flux and plasma power dissipation can be described by a power balance equation: Following Misium *et al* ,[40] the rf power P_p dissipated in the plasma is distributed between electron collisions, the ion flux power $2\Gamma(e\overline{V_p})$, and the electron flux power $2\Gamma(4kT_e)$ per unit area to both electrodes (the time-averaged ion and electron flux Γ are equal to maintain

quasi-neutrality). Each ion represents an energy loss of $e\overline{V_p}$ even though charge exchange means that most ions do not arrive with the full sheath energy - the energy deficit of the final ion appears as gas heating by production of fast neutrals. The electron collision term includes ionisation, excitation and elastic collisions which can be combined by defining an average collision energy $\varepsilon_{coll}(T_e)$ per electron.[40] The total power balance per unit electrode area is therefore:

$$P_p = \Gamma\left(2e\overline{V_p} + 8kT_e + \varepsilon_{coll}(T_e)\right) = \Gamma\left(2e\overline{V_p} + F(T_e)\right) \qquad (5)$$

where $F(T_e)$ is the total electron energy dissipated per electron-ion pair created. Since $\overline{V_p}$ is a constant for each curve in Fig. 8, and insofar as T_e can be taken to be independent of frequency (see Section III.B and Refs. 5 and 6) to a first order approximation, this gives the ion flux Γ approximately proportional to the rf power P_p. This simplified description therefore yields a qualitative agreement for the frequency dependence of the flux ($f^{2.1\pm0.2}$) in terms of the rf power dependence ($f^{2.4\pm0.2}$ from Eq. (4) with $V_{rf}/2 \approx \overline{V_p}$ = constant). The increased discharge power factor, due to reduced sheath impedance at high frequencies with consequently higher discharge rf currents for the same V_{rf}, is at the physical origin of the higher ion flux and rf power.

Improved deposition rates at constant rf power in VHF plasmas[1,3,6] (and therefore with lower ion energy[3,6] - see Fig. 5) may be in part due to an increased fraction of the rf power in the electron dissipation term $F(T_e)$ of Eq.(5), yielding higher dissociation rates at the expense of proportionately less ion flux power.[5] The question is further complicated by various issues such as enhanced dehydrogenisation at the surface of the growing film[18,19] due to higher ion bombardment flux in VHF plasmas[6]; this is beyond the scope of the present study.

Figs. 3, 5 and 8 demonstrate the possibility of controlling the ion energy and flux via the rf frequency and power.[5,12] Once the rf electrode voltage V_{rf} has been determined to give the required maximum ion energy (using Fig. 3), the

required ion flux can be chosen by varying the excitation frequency (and power) as in Fig. 8. The technical difficulty of variable frequency operation applies only to the pilot reactor because once the excitation frequency has been chosen to optimise a given process, subsequent plasma processing reactors need only operate at this fixed frequency.

D. Sheath width and ion density as a function of rf frequency

The ion flux at the electrode Γ equals the ion flux entering the sheath from the bulk plasma (excepting any ionisation in the sheath region). Ions from the bulk plasma enter the sheath with velocity $\sqrt{kT_e/m_i}$, satisfying the Bohm criterion, and so the strong increase in ion flux with frequency shown in Fig. 8 represents a parallel increase in plasma ion density[5,12] (provided that T_e does not change strongly with frequency[6]). The ion density just in front of the electrode, n_{is}, also increases with frequency albeit less strongly than the flux because of the frequency-dependence of the distribution function shown in Fig. 6.

The time-averaged charge density $e(n_i - \overline{n_e})$ throughout the sheath is approximately constant[17] and equal to n_{is} because the time-averaged electron density $\overline{n_e}$ is negligible near the electrode surface. Poisson's equation integrated across the time-averaged sheath width d_s therefore gives:

$$d_s = \sqrt{\left(2\varepsilon_o \overline{V_p}/en_{is}\right)}. \qquad (6)$$

It follows that the sheath for constant electrode voltage is thinner at high frequencies, in agreement with Fig. 7 and simulations,[12-14] due to an increase in sheath ion density. Similar considerations for VHF plasmas at constant rf power also show thinner sheaths,[6,8,16,17] principally due to lower values of $\overline{V_p}$ (see Fig. 5) in Eq.(6).

In summary, the reduction in sheath impedance $1/\omega C$ at high frequency is responsible for a higher power factor, leading to higher ion fluxes and ion density for a given plasma potential, which in turn reduces the sheath width (by Eq.(6)) and increases the sheath capacitance; this accentuates the effectiveness of

the frequency (as mentioned in Section III.B) by reducing the sheath impedance still further. Coincidental advantages associated with thinner sheaths are improved ion flux uniformity,[5,13] a shorter path length for reactive radicals from the plasma bulk to the substrate,[8] and improved ion directionality due to reduced scattering.[5,12,13,41]

IV. CONCLUSIONS

The frequency dependence (f = 13.56 MHz to 70 MHz) of the ion energy distribution in a symmetrical argon discharge was used to investigate the inherent properties of Very High Frequency plasmas.

Ion energy measurements and a Particle-In-Cell simulation show that the sheaths are capacitive. Independently of the frequency, the maximum ion energy (in eV) is approximately half of the rf voltage amplitude except at the lowest voltages where the minimum ion energy range is determined by the floating potential ($V_f \approx 5\,kT_e/e$).

At high frequencies, the reduced impedance of the capacitive sheaths raises the discharge power factor, and the measured ratio (rf power)/(electrode voltage)^2 varies approximately as $f^{2.4}$. Significant rf power can therefore be applied at low rf voltages thereby maintaining the ion bombardment energy near to the minimum value. At constant electrode voltage, the measured ion flux increases approximately as $f^{2.2}$. This is qualitatively explained by the increase in rf power with frequency, as shown by consideration of the electron and ion power balance in the plasma. The ion flux and energy can therefore be independently controlled by appropriate choice of the rf voltage and frequency, as shown in simulations by other authors.[5,12,13]

The capacitive sheaths are thinner at high frequencies due to the combination of higher ion density and/or reduced sheath voltage, which accentuates the effectiveness of Very High Frequency operation by reducing the sheath impedance still further.

In conclusion, it has been shown that diminished sheath impedance is reponsible for several intrinsic advantages of Very High Frequency plasma deposition such as high ion density, thin sheaths, and high ion flux with low ion energy at the substrate.

ACKNOWLEDGMENTS

The authors gratefully acknowledge Professor A. Shah and his group at IMT Neuchâtel for their advice and motivation for this work. They also thank Professor C. K. Birdsall for providing his XPDP1 code, and A. Gunzinger and colleagues for access to the MUSIC parallel supercomputer. This work was funded by Swiss Federal Grant ENET 9400051.

REFERENCES:

[1]H. Curtins, N. Wyrsch, M. Favre and A. V. Shah, Plasma Chem. Plasma Processing **7**, 267 (1987).

[2]M. Moisan, C. Barbeau, R. Claude, C. M. Ferreira, J. Margot, J. Paraszczak, A. B. Sá, G. Sauvé, and M. R. Wertheimer, J. Vac. Sci. Technol. B **9**, 8 (1991).

[3]A. A. Howling, J.-L. Dorier, Ch. Hollenstein, U. Kroll, F. Finger, J. Vac. Sci. Technol. A **10**, 1080 (1992).

[4]F. Finger, U. Kroll, V. Viret, A. Shah, W. Beyer, X.-M. Tang, J. Weber, A. Howling, and Ch. Hollenstein, J. Appl. Phys. **71**, 5665 (1992).

[5]M. J. Colgan, M. Meyyappan, and T. R. Govindan, Electrochem. Soc. 10th Symp. on Plasma Processing, May 1994.

[6]M. Heintze, R. Zedlitz, and G. H. Bauer, J. Phys. D: Appl. Phys. **26**, 1781 (1993).

[7]K. M. Kalpakjian, M. A. Lieberman, and W. G. Oldham, J. Vac. Sci. Technol. B **12**, 1351 (1994).

[8]U. Kroll, Y. Ziegler, J. Meier, H. Keppner and A. Shah, Mat. Res. Soc. Symp. Proc. **336**, 115 (1994).

[9]F. Finger, P. Hapke, M. Luysberg, R. Carius, H. Wagner, and M. Scheib, Appl. Phys. Lett. **65**, 2588 (1994).

[10]J. Meier, R. Flückiger, H. Keppner, and A. Shah, Appl. Phys. Lett. **65**, 860 (1994).

[11]D. L. Flamm, J. Vac. Sci. Technol. A **4**, 729 (1986).

[12]M. Surendra and D. B. Graves, Appl. Phys. Lett. **59**, 2091 (1991).

[13]V. Vahedi, C. K. Birdsall, M. A. Lieberman, G. DiPeso, and T. D. Rognlien, Phys. Fluids B **5**, 2719 (1993).

[14]M. J. Colgan, M. Meyyappan, and D. E. Murnick, Plasma Sources Sci. Technol. **3**, 181 (1994).

[15]J. Dutta, U. Kroll, P. Chabloz, A. Shah, A. A. Howling, J.-L. Dorier, and Ch. Hollenstein, J. Appl. Phys. **72**, 3220 (1992).

[16]C. Beneking, J. Appl. Phys. **68**, 4461 (1990).

[17]M. Fivaz, S. Brunner, W. Schwarzenbach, A. A. Howling, and Ch. Hollenstein, accepted for publication in Plasma Sources Sci. Technol.

[18]S. Veprek, F.-A. Sarrott, S. Rambert, and E. Taglauer, J. Vac. Sci. Technol. A **7**, 2614 (1989).

[19]J. Perrin, Y. Takeda, N. Hirano, H. Matsuura, and A. Matsuda, Jap. J. Appl. Phys. **28**, 5 (1989).

[20]P. H. Singer, Semicond. Int. **15**, 78 (1992).

[21]K. Köhler, J. W. Coburn, D. E. Horne, E. Kay, and J. H. Keller, J. Appl. Phys. **57**, 59 (1985).

[22]K. Köhler, D. E. Horne, and J. W. Coburn, J. Appl. Phys. **58**, 3350 (1985).

[23]C. M. Ferreira and M. Moisan, Physica Scripta **38**, 382 (1988).

[24]P. M. Meijer, J. D. P. Passchier, W. J. Goedheer, J. Bezemer, and W. G. J. H. M. van Sark, Appl. Phys. Lett. **64**, 1780 (1994).

[25]C. K. Birdsall, IEEE Trans. Plasma Sci. **PS-19**, 65 (1991).

[26]Hiden Analytical Limited, Gemini Business Park, Warrington WA5 5TN, UK.

[27]W. D. Davis, T. A. Vanderslice, Phys. Rev. **131**, 219 (1963).

[28]C. Wild and P. Koidl, J. Appl. Phys. **69**, 2909 (1991).

[29]A. Garscadden and K. G. Emeleus, Proc. Phys. Soc. **79**, 535 (1962).

[30]H. S. Butler and G. S. Kino, Phys. Fluids **6**, 1346 (1963).

[31]K.-U. Riemann, J. Appl. Phys. **65**, 999 (1989).

[32]Y. Wang, Appl. Phys. Lett. **66**, 2186 (1995).

[33]B. Chapman, *Glow Discharge Processes*, John Wiley & Sons (1980) p69.

[34]M. A. Lieberman, IEEE Trans. Plasma Sci. **16**, 638 (1988).

[35]A. M. Pointu, Appl. Phys. Lett. **50**, 316 (1987).

[36]V. A. Godyak, R. B. Piejak, and B. M. Alexandrovich, J. Appl. Phys. **69**, 3455 (1991).

[37]C. Böhm, PhD thesis, Ecole Polytechnique de Palaiseau, 1992.

[38]V. A. Godyak, R. B. Piejak, J. Vac. Sci. Technol. A **8**, 3833 (1990).

[39]B. Andries, G. Ravel, and L. Peccoud, J. Vac. Sci. Technol. A **7**, 2774 (1989).

[40]G. R. Misium, A. J. Lichtenberg, and M. A. Lieberman, J. Vac. Sci. Technol. A **7**, 1007 (1989).

[41]M. J. Kushner, J. Appl. Phys. **58**, 4024 (1985).

FIGURE CAPTIONS

Fig. 1 Schematic of the reactor and mass spectrometer. The inset shows the cylindrical electrodes, concentric screens, mass spectrometer orifice and extraction electrode. The rf voltage and self-bias were measured by the voltage probe on the back face of the rf electrode. The rf screen height H (16 mm) was adjusted to obtain zero self-bias.

Fig. 2 Energy distribution of the Ar^+ flux at the ground electrode by Particle-In-Cell simulation and experiment. The measured ArH^+ energy spectrum is also shown. The maximum ion energy by experiment was taken to be 60 eV. Excitation frequency 25 MHz with 3 W power in the plasma.

Fig. 3 The maximum ion energy at the ground electrode as a function of rf electrode voltage V_{rf}. The range of electrode voltage was covered by using different excitation frequencies with rf powers between 1 and 14 W (see Fig. 4). The full curve was calculated according to Eq. (2) with kT_e/e = 3 eV and V_f = 16 V. The PIC data were obtained for frequencies 25 to 70 MHz for rf powers 3 W and 7 W.

Fig. 4 (a) The electrode voltage and corresponding plasma power ranges for several of the frequencies used in Fig. 3; and (b) frequency power-law scaling of the ratio V_{rf}^2/P_p for all experimental data points shown in Fig. 3.

Fig. 5 Frequency scaling of the rf voltage and maximum ion energy (by experiment and simulation) for a constant rf plasma power of 3 W.

Fig. 6 Ar^+ ion flux energy distributions, normalised to the total flux at each frequency, obtained by adjusting the rf power at each frequency in order to obtain the same maximum ion energy (29 eV in this figure).

Fig. 7 Ratio of sheath width to charge exchange mean free path (approximately 0.5 mm at 0.1 Torr) obtained by fitting the Davis and Vanderslice[27] distribution function to the curves in Fig. 6. The mean ion energy of the corresponding distributions for a fixed maximum ion energy of 29 eV is also shown for different excitation frequencies.

Fig. 8 Measured frequency dependence of the total ion flux for constant maximum ion energies of 29 eV (the normalised distribution functions are shown in Fig. 6) and 39 eV. The curves represent power-law fits to the experimental data points.

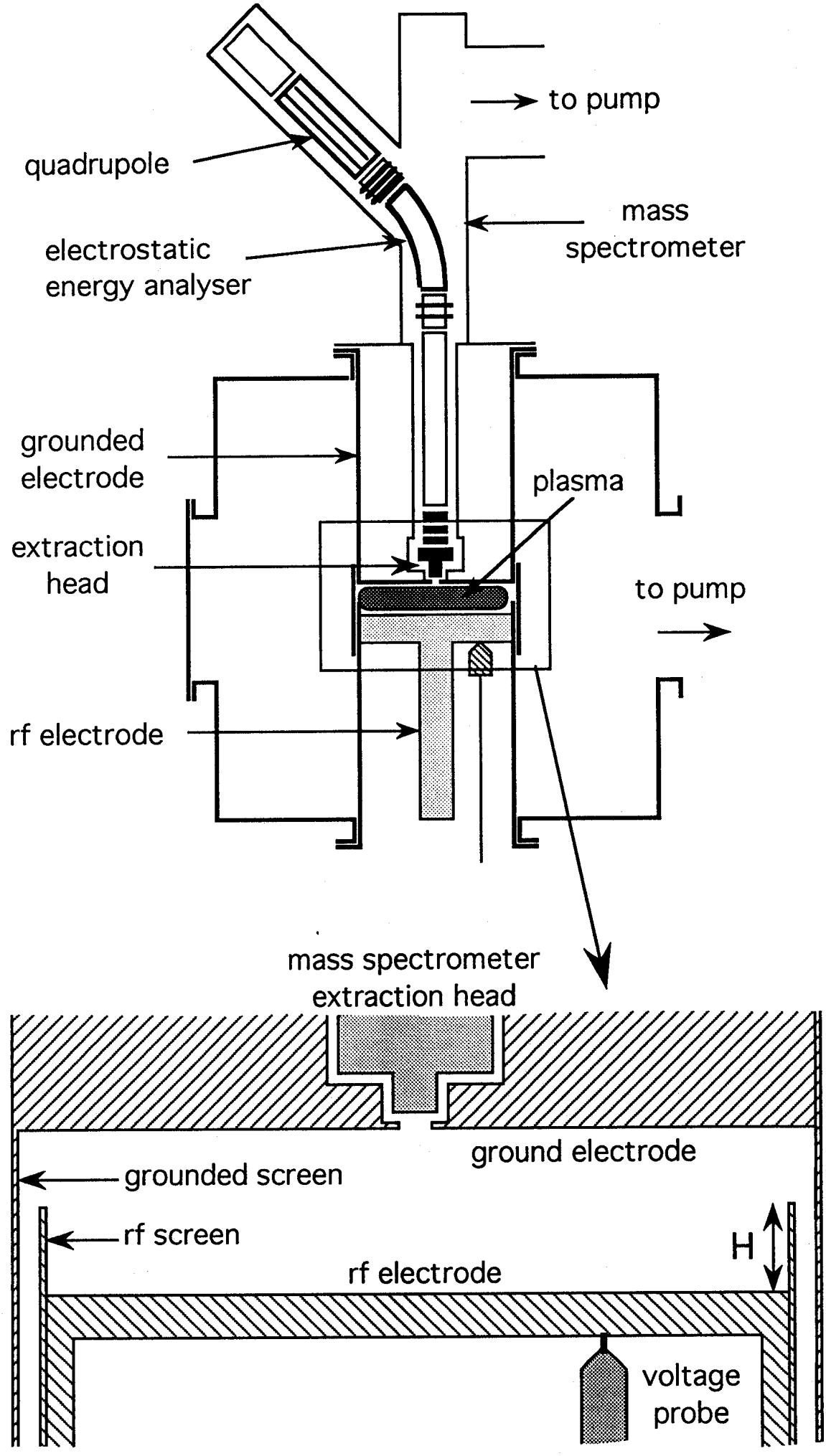
to pump
quadrupole
mass
spectrometer
electrostatic
energy analyser
grounded
electrode
plasma
extraction
head
to pump
rf electrode
mass spectrometer
extraction head
ground electrode
grounded screen
rf screen
H
rf electrode
voltage
probe

FIGURE 1

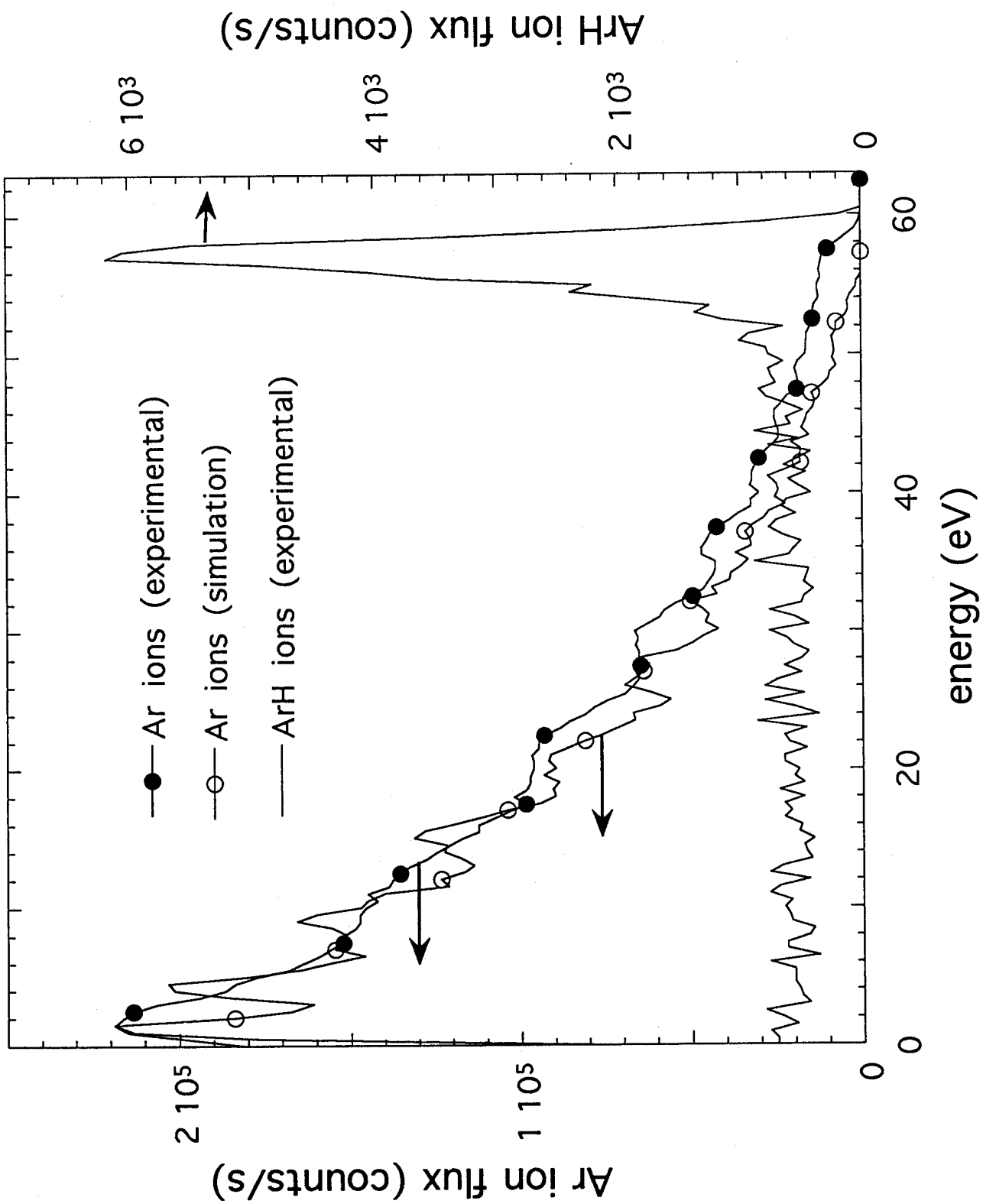
Ar ion flux (counts/s)
2 10^5
1 10^5
0
ArH ion flux (counts/s)
6 10^3
4 10^3
2 10^3
0
0
20
40
60
energy (eV)
Ar ions (experimental)
Ar ions (simulation)
ArH ions (experimental)

FIGURE 2

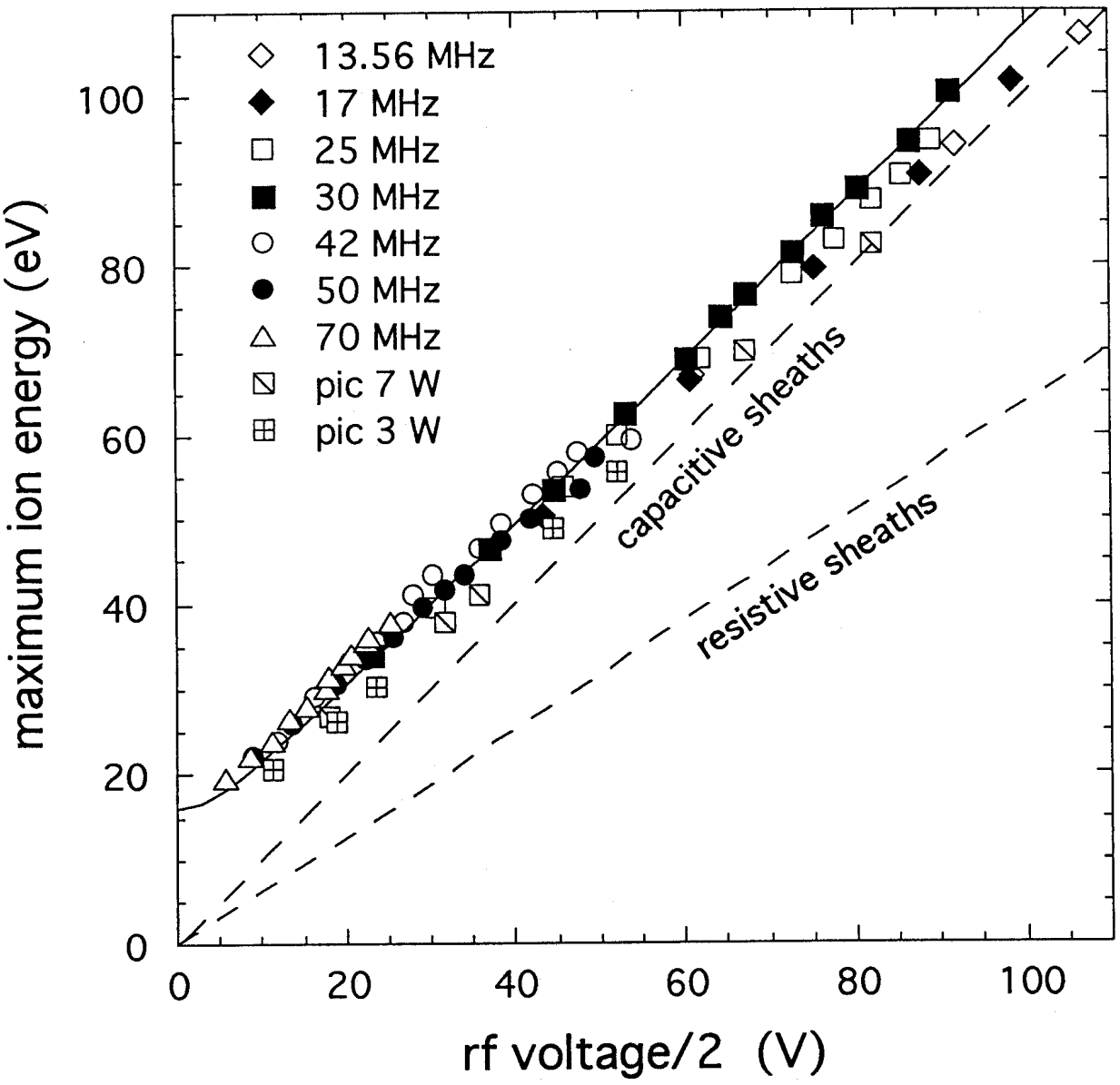
13.56 MHz
17 MHz
25 MHz
30 MHz
42 MHz
50 MHz
70 MHz
pic 7 W
pic 3 W
capacitive sheaths
resistive sheaths
maximum ion energy (eV)
rf voltage/2 (V)
0
20
40
60
80
100

FIGURE 3

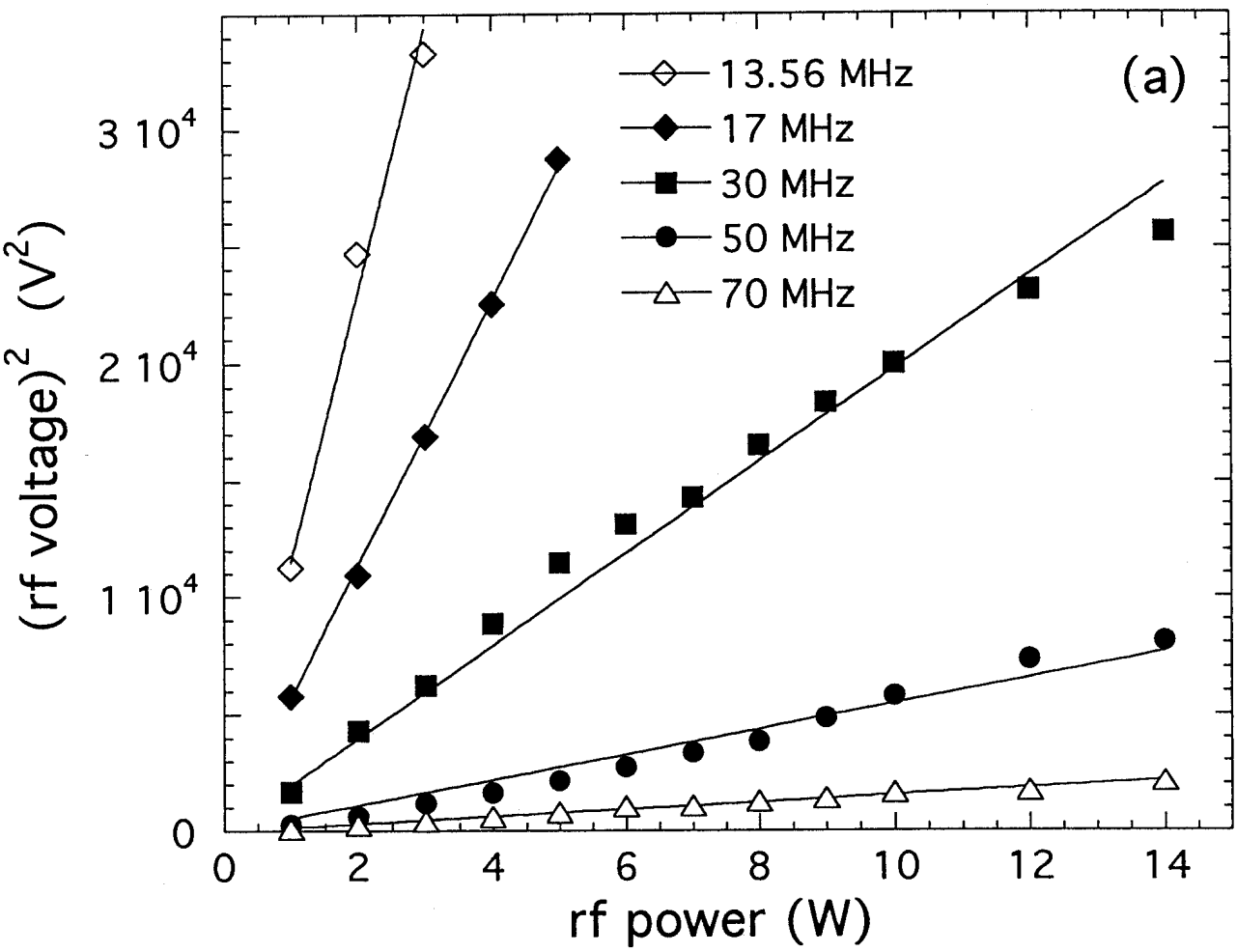
13.56 MHz
17 MHz
30 MHz
50 MHz
70 MHz
(a)
3 10^4
2 10^4
1 10^4
0
(rf voltage)^2 (V^2)
0
2
4
6
8
10
12
14
rf power (W)

FIGURE 4(a)

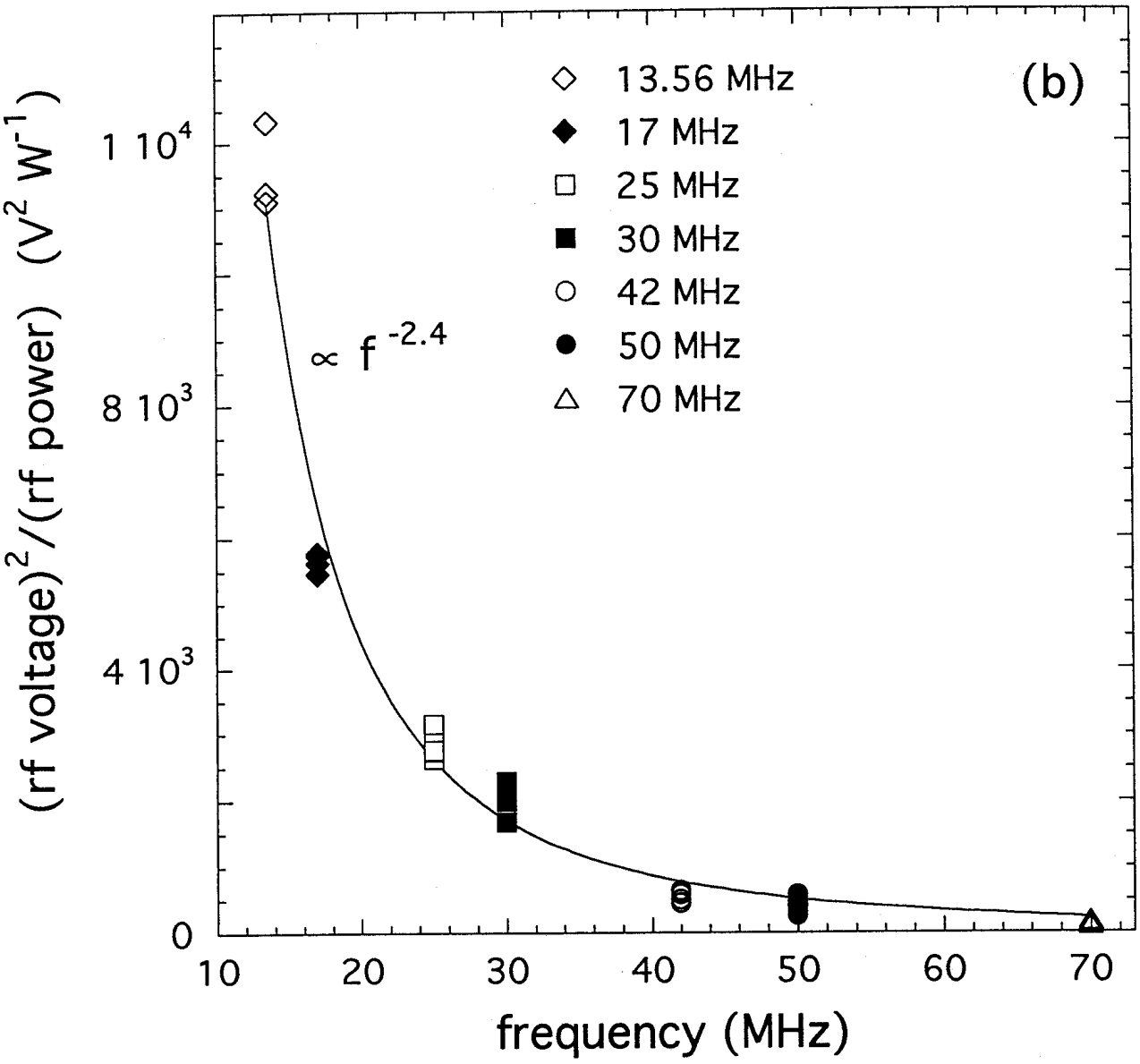
(b)
13.56 MHz
17 MHz
25 MHz
30 MHz
42 MHz
50 MHz
70 MHz
∝ f -2.4
(rf voltage)2/(rf power) (V2 W-1)
1 10^4
8 10^3
4 10^3
0
10
20
30
40
50
60
70
frequency (MHz)

FIGURE 4(b)

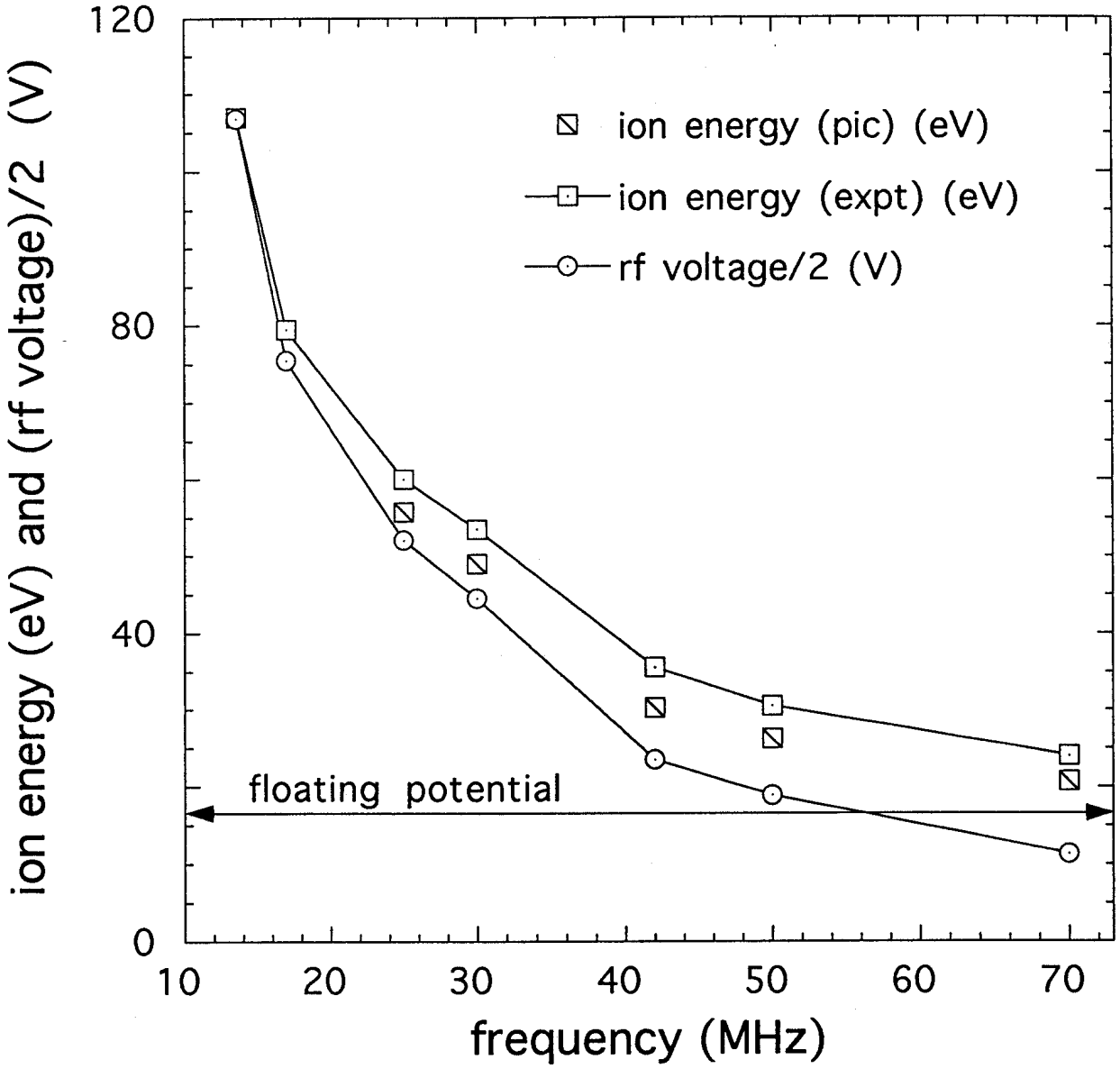
120
80
40
0
10
20
30
40
50
60
70
ion energy (eV) and (rf voltage)/2 (V)
frequency (MHz)
ion energy (pic) (eV)
ion energy (expt) (eV)
rf voltage/2 (V)
floating potential

FIGURE 5

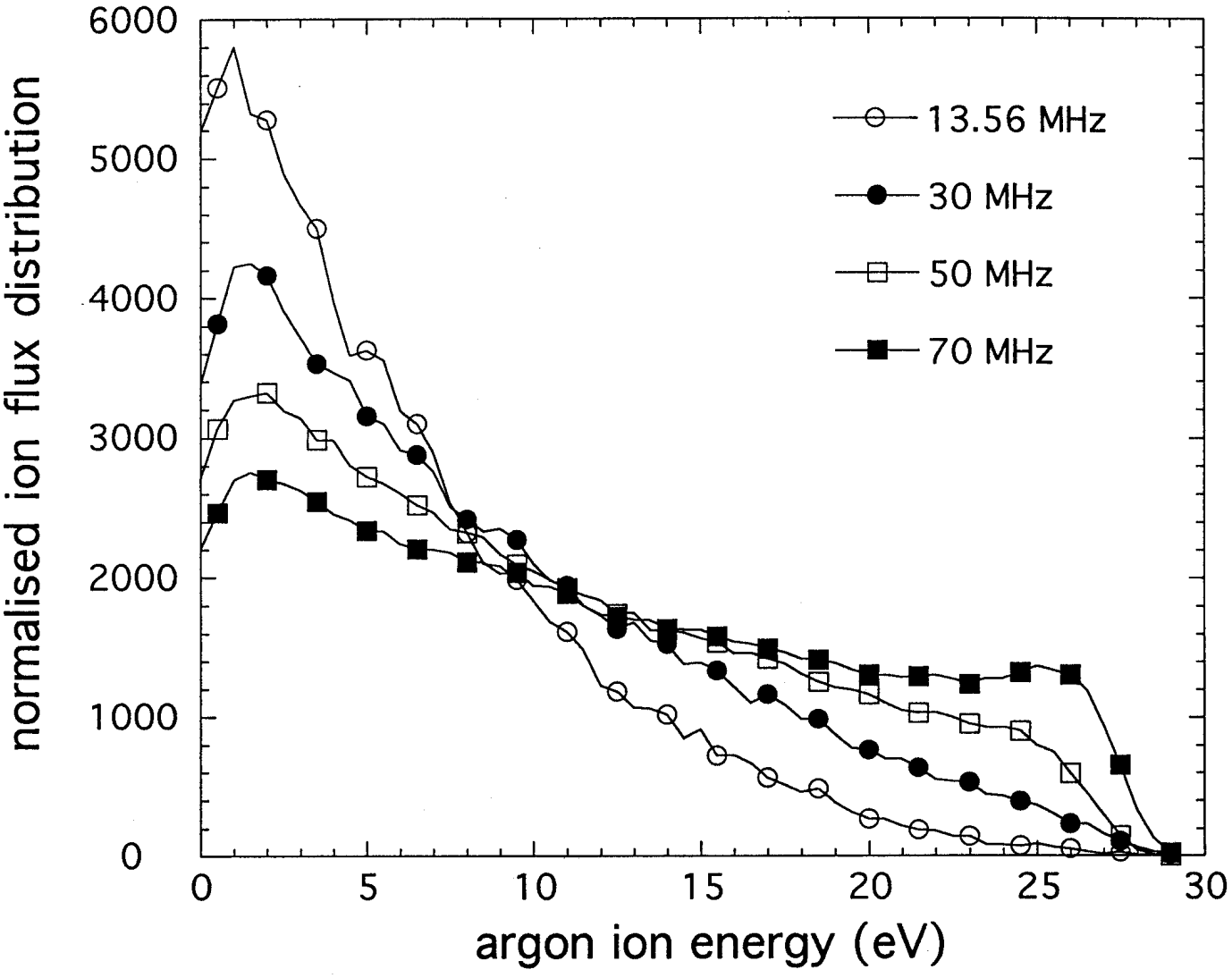
normalised ion flux distribution
6000
5000
4000
3000
2000
1000
0
0
5
10
15
20
25
30
argon ion energy (eV)
13.56 MHz
30 MHz
50 MHz
70 MHz

FIGURE 6

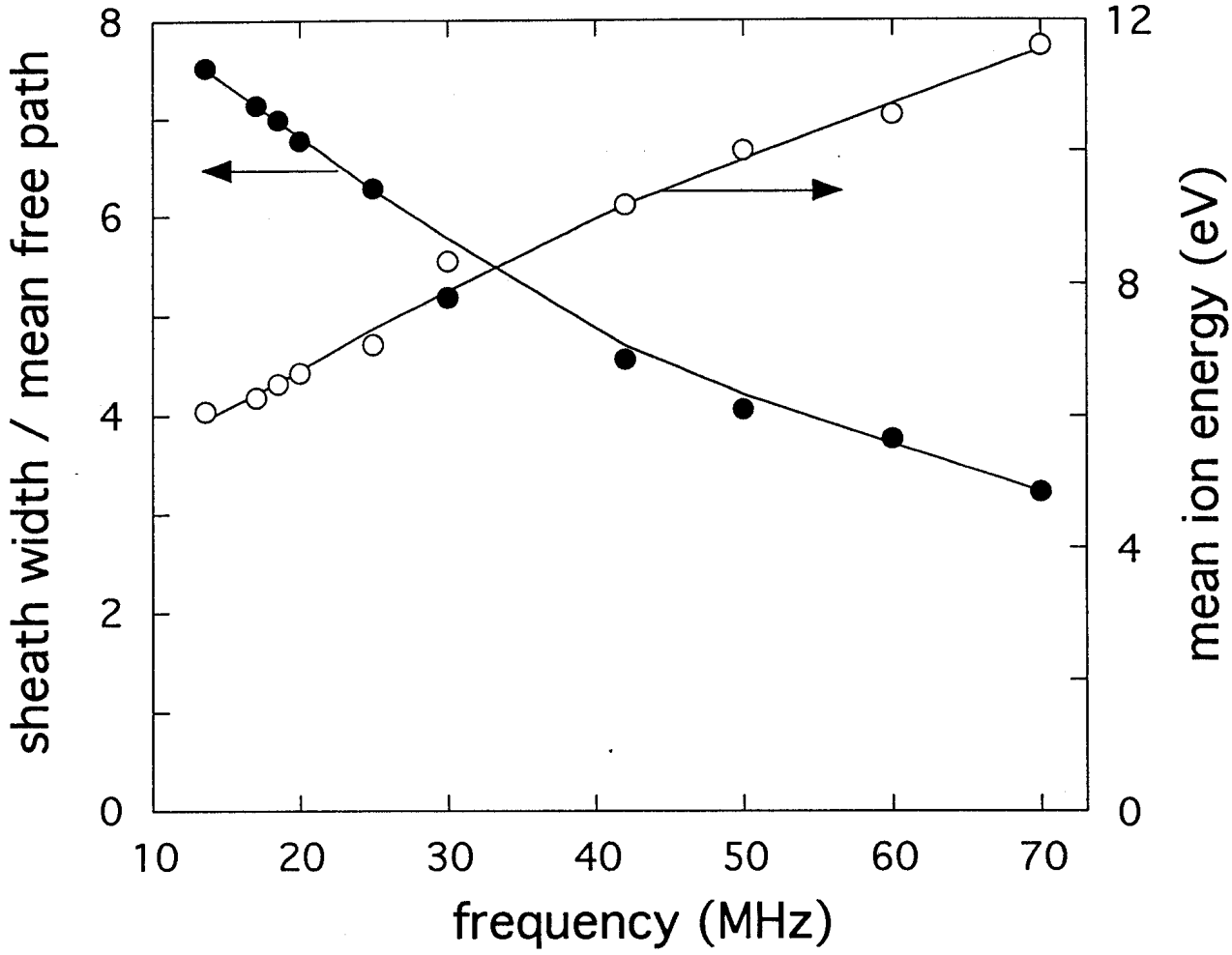
sheath width / mean free path
mean ion energy (eV)
frequency (MHz)
0
2
4
6
8
0
4
8
12
10
20
30
40
50
60
70

FIGURE 7

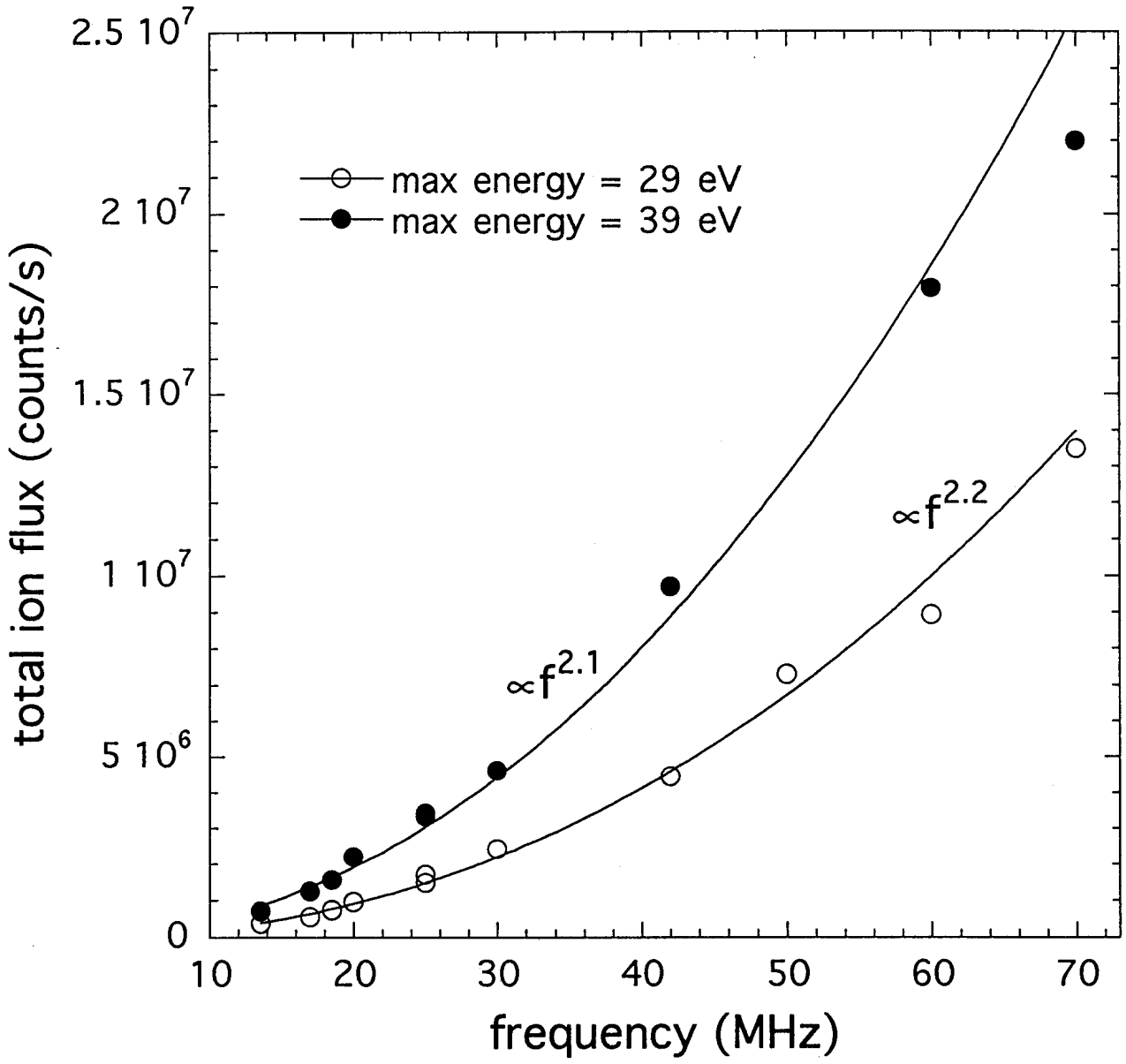
2.5 10^7
2 10^7
1.5 10^7
1 10^7
5 10^6
0
total ion flux (counts/s)
max energy = 29 eV
max energy = 39 eV
∝f^2.1
∝f^2.2
10
20
30
40
50
60
70
frequency (MHz)

FIGURE 8